ELSEVIER

Chemical Engineering Journal 71 (1998) 11–21

Chemical Engineering Journal

# Flow generated by a disc turbine in aqueous solutions of polyacrylamide

V.P. Mishra, P. Kumar, J.B. Joshi*

*Department of Chemical Technology, University of Mumbai, Matunga, Mumbai, 400 019, India*

Received 2 December 1996; received in revised form 15 May 1998; accepted 3 June 1998

**Abstract**

The flow generated by a disc turbine in aqueous solutions of polyacrylamide (PAA) (molecular weight: $5 \times 10^6$–$6 \times 10^6$) in a cylindrical tank was measured using laser Doppler anemometry. The tank diameter was 300 mm, with a flat bottom and provided with four *T*/10 baffles. The disc turbine was 100 mm in diameter and was centrally located. The liquid height was kept equal to the vessel diameter. The effect of polymer concentration on the flow was investigated for the same impeller speed. Results obtained were compared with those where only water was used as the flow medium. The effect of the impeller speed was also investigated for a polymer concentration of 5000 ppm. Dimensionless mean velocities were found to be independent of the impeller speed in the impeller vicinity. The primary, secondary flow numbers and power numbers decreased with an increase in the polymer concentration. The values of maximum shear rates were estimated in the impeller region as well as bulk region. On this basis, Reynolds number have been reported. They were found to be in qualitative agreement with the Reynolds number obtained by Metzner–Otto correlation. A procedure has been given for the estimation of turbulent energy dissipation rate. A complete energy balance has been established for the case of turbulent flow. The turbulent energy dissipation rates were also determined for the polymer solutions where the flow was in the transition regime. 

*Keywords:* Disc turbine; Polyacrylamide; Laser doppler anemometry

## 1. Introduction

The present paper described the power consumption characteristics and the flow generated by a disc turbine in aqueous solutions of polyacrylamide (PAA). Hoyt [1], Virk [2] and White and Hemings [3] have critically reviewed the literature on the flow of polymer solutions through conduits and the external flows past regularly shaped bodies. Pinho and Whitelaw [4] have reported measurements of mean axial velocity and three normal stresses in fully developed pipe flows with four concentrations of carboxymethyl cellulose (CMC) in aqueous solution and with water and viscous Newtonian fluids. A delay in the transition from laminar to turbulent flow due to shear thinning, suppression of turbulent normal stresses and drag reduction at higher Reynolds numbers have been quantified. Pinho and Whitelaw [5] have also measured wall pressure, mean and rms velocities of the confined flow about a disk of 50% area blockage for four concentrations of CMC. At the same Reynolds number, it was observed that the turbulent kinetic energy decreases with an increase in the CMC concentration. For instance, at a Reynolds number of 8000, the maximum value of turbulent kinetic energy was 35 and 45% lower than that for water at 0.2 and 0.4% CMC solution, respectively. Rudd [6] has presented useful data for the case of pipe flow. The author has been able to show that the thickness of viscous sublayer increases when 100 ppm of polyacrylamide was added to water. The rms velocities also increase near the wall.

For the last 15 years, substantial information has been reported in the published literature on the flow generated by different impeller designs. However, in most of the cases water was used as the medium. Therefore, it was thought desirable to undertake systematic investigation of flows generated by a disc turbine in aqueous solutions of polyacrylamide.

## 2. Experimental

The experimental system was composed of an agitator assembly, a flat bottomed cylindrical vessel (i.d., $T = 0.3$,

*Corresponding author. Fax: +91-022-4145614; e-mail: jbj@udct.ernet.in

1385-8947/98/$ – see front matter 
PII: S1385-8947(98)00112-0

height $H = T$) made up of perspex, provided with four baffles of width $T/10$. To minimise the effect of curvature on the intersecting beams, the vessel was placed inside a square vessel. A standard disc turbine ($D = 0.1$) was used as the impeller. The impeller was centrally located and driven by a variable speed DC motor. The flow was measured using DANTEC 55X modular series laser Doppler anemometer (LDA), 57 N 10 burst spectrum analyser (BSA) provided with fast Fourier tranform module and a personal computer. The LDA was used in the forward scatter mode. The mean velocities and rms fluctuating velocities were statistically determined. The sample size was verified as satisfactory as to achieve 1% reproducibility. Further details pertaining to the experiments are given by Ranade and Joshi [7]. Radial and axial mean and rms velocities were measured. The velocities reported in this work are dimensionless, obtained by dividing the real values by the impeller tip speed, $V_t$. High molecular weight polyacrylamide (molecular weight $= 5 \times 10^6$–$6 \times 10^6$) was used as the polymer. Water solutions of polymer were made at room temperature. Polymer solution viscosities and normal forces (under sheared flow conditions, the maximum shear rate - $= 100\ s^{-1}$) were measured with the help of a disc and plate RHEOMETRICS RECAP II – RMS 800 viscometer. The results are given in Table 1. It can be seen that the polymer solutions are shear thinning. Further, from the information on normal stress difference, the solutions are viscoelastic.

Table 1
Viscosity and normal stress under sheared conditions (geometry: disc and plate, diameter: 25 mm)

| PAA concentration in water | Shear rate ($s^{-1}$) | Apparent viscosity (Pa s) | Normal stress difference (Pa) |
|---|---|---|---|
| 2000 ppm Gap = 1.87 mm | 0.00100 | 8.7150 | 11.43 |
| | 0.00215 | 2.2630 | 25.58 |
| | 0.00464 | 0.6300 | 38.16 |
| | 0.01000 | 0.3540 | 50.33 |
| | 0.02150 | 0.3190 | 61.93 |
| | 0.04640 | 0.2680 | 73.04 |
| | 0.10000 | 0.1380 | 83.68 |
| | 0.21500 | 0.0640 | 94.56 |
| | 0.46400 | 0.0520 | 104.3 |
| | 0.99900 | 0.0270 | 112.9 |
| | 2.15000 | 0.0150 | 121.2 |
| | 4.64000 | 0.0066 | 129.2 |
| | 9.99000 | 0.0034 | 136.3 |
| | 21.5400 | 0.0023 | 143.5 |
| | 46.4000 | 0.0014 | 151.9 |
| | 100.000 | 0.0025 | 166.0 |
| 5000 ppm Gap = 1.42 mm | 0.0010 | 15.040 | 18.25 |
| | 0.00215 | 9.0700 | 37.64 |
| | 0.00464 | 5.1500 | 57.00 |
| | 0.01000 | 3.1300 | 76.38 |
| | 0.02150 | 1.7000 | 94.55 |
| | 0.04640 | 0.1940 | 110.8 |
| | 0.10000 | 0.1890 | 126.3 |
| | 0.21500 | 0.0300 | 140.6 |
| | 0.46400 | 0.0110 | 153.3 |
| | 0.99900 | 0.0076 | 163.8 |
| | 2.15000 | 0.0017 | 173.3 |
| | 4.64000 | 0.0066 | 182.1 |
| | 9.99000 | 0.0095 | 190.3 |
| | 21.5400 | 0.0111 | 197.8 |
| | 46.4000 | 0.0111 | 205.7 |
| | 100.000 | 0.0095 | 216.9 |
| 10 000 ppm Gap = 1.08 mm | 0.00100 | 10.14 | 140.4 |
| | 0.00215 | 3.2220 | 146.7 |
| | 0.00464 | 1.4280 | 151.4 |
| | 0.01000 | 0.4703 | 154.9 |
| | 0.02150 | 0.2978 | 156.6 |
| | 0.04640 | 0.1462 | 157.2 |
| | 0.10000 | 0.0841 | 156.5 |
| | 0.21500 | 0.1090 | 154.4 |
| | 0.46400 | 0.0883 | 151.0 |
| | 0.99900 | 0.0704 | 149.8 |
| | 2.15000 | 0.0651 | 148.0 |
| | 4.64000 | 0.0599 | 146.8 |
| | 9.99000 | 0.0534 | 145.2 |
| | 21.5400 | 0.0459 | 142.7 |
| | 46.4000 | 0.0394 | 139.0 |
| | 100.000 | 0.0320 | 134.8 |

## 3. Results and discussion

### 3.1. Effect of polymer concentration

To study the effect of polymer concentration on the flow generated by a disc turbine, polymer solutions of three different concentrations, viz., 2000, 5000 and 10 000 ppm were made. For the purpose of comparison, measurements were also made using water (zero polymer concentration). The range of Reynolds number is given in Table 2. In the present work, we have measured axial and radial velocities with respect to axial and radial locations. Therefore, it is possible to estimate the components of shear rates. We have considered two possibilities and estimated maximum values of $\partial U/\partial z$ in the impeller region and in the bulk region. These estimations resulted into two values of apparent viscosity. In addition, we also calculated the apparent viscosity using Metzner–Otto correlation. For this case, we assumed that the shear rate equals 10 N (Eq. (8)). Thus, we get three values of Reynolds numbers that are reported in Table 2. It can be seen that the range of Reynolds number is practically the same in all the three cases.

Alternatively, we thought it desirable to use measured radial velocity in place of ND (which is the usual representation for velocity in Reynolds number). The resulting values of Reynolds number $UD\rho/\mu_a$) were calculated in the impeller region and bulk region and given in Table 2.

#### 3.1.1. Flow in the impeller vicinity

Axial profiles of the radial velocity at a radial distance $r = R_i + 3$ mm are shown in Fig. 1. The radial velocities decrease with an increase in the polymer concentration owing to a decrease in the Reynolds number. At all the

Table 2
Flow characteristics in terms of primary and secondary flow numbers and Reynolds number (Impeller speed = 4.5 r $s^{-1}$)

| PAA concentration in water (ppm) | Primary flow number ($QN/D^3$) | Secondary flow number ($Q_s/ND^3$) | Reynolds number | | | | |
|---|---|---|---|---|---|---|---|
| | | | $D^2N\rho/\mu_a$ M–O approach | $D_2N\rho/\mu_a$ from LDA measurements on the basis of maximum shear rate | | $DU\rho/\mu_a$ from LDA measurements on the basis of maximum radial velocity | |
| | | | | IR | BR | IR | BR |
| 0 (water) | 0.78 | 0.86 | 45 000 | 45 000 | 45 000 | 98 980 | 4242 |
| 2000 | 0.64 | 0.66 | 32 142 | 18 292 | 8571 | 37361 | 1696 |
| 5000 | 0.58 | 0.59 | 4068 | 4726 | 5625 | 8911 | 2651 |
| 10 000 | 0.52 | 0.53 | 1142 | 1404 | 789 | 1873 | 298 |

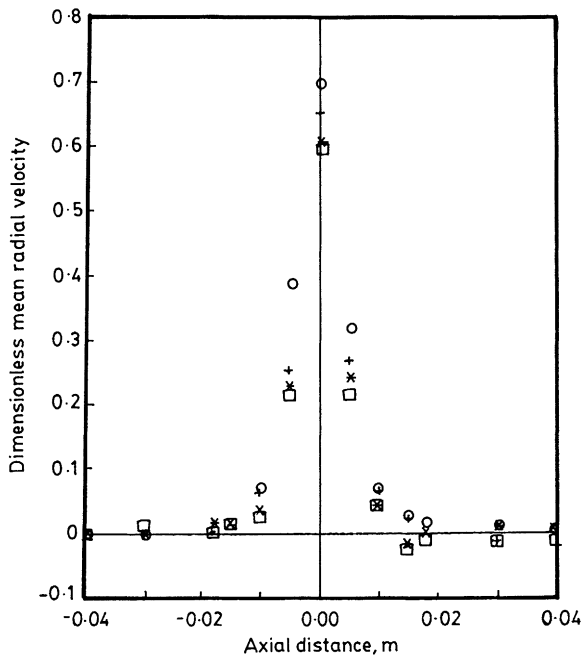


Fig. 1. Axial profile of mean radial velocity at $r = R_i + 3$ mm Symbols: (○), water; (+), 2000 ppm PAA; (∗), 5000 ppm PAA; (□), 10 000 ppm PAA (See Figs. 1–9).

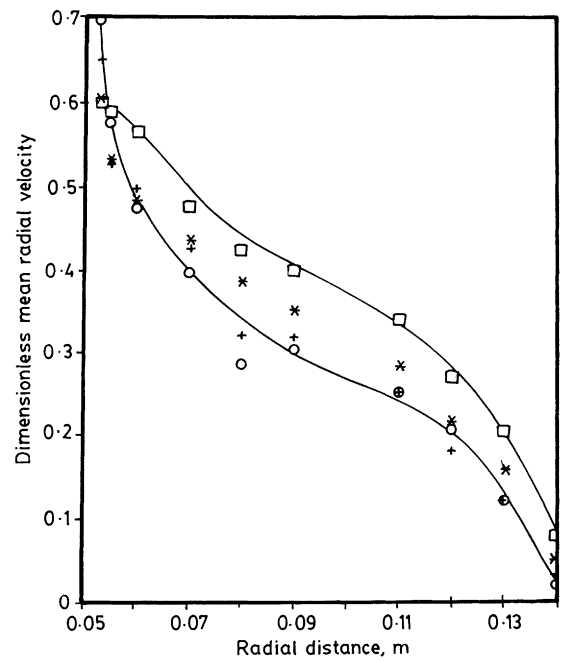


Fig. 2. Radial profile of mean radial velocity at $z$=0.

concentrations, maxima occur along the impeller centre plane and the profiles are symmetrical. The maximum radial velocity close to the impeller tip is $0.7V_t$ for water and $0.6V_t$ for the highest concentration solution. Though, with an increase in the polymer concentration there is a reduction in the magnitude of radial velocities, the nature of profiles remains similar to that of water. Along the impeller centre plane, (Fig. 2, $z = 0$) as in the case of water, the radial velocities decrease with increasing radius. Away from the impeller tip, the radial velocities are higher at high polymer concentration. At all the concentrations, the radial flow extends upto the vessel wall. Inradial planes above ($z = 0.36R_i$, Fig. 3(A)) and below ($z = -0.36R_i$ the impeller centre line, the radial velocities are high between $r = 2R_i$ to $2.4R_i$. Also, the velocities decrease with an increase in concentration. This indicates widening of the main radial discharge streams in the case lower concentration solutions and water. That is, in the highest concentration solution, the narrowness of the radial discharge jet is the reason for the higher radial velocities along the impeller centre plane. The measurement of average resultant length scale in the impeller centre plane also confirms the narrowness of the radial discharge stream in case of highest concentration solution. The average resultant length scale for water, 2000 and 5000 ppm are 2.02, 2.22 and 2.11 cm, respectively, whereas for 10 000 ppm solution it is only 1.78 cm. It can be seen from Fig. 3(A) that except near $r = R_i$, the flow is towards the vessel wall in all the cases. Rms velocities along the impeller centre plane ($z = 0$) are shown in Fig. 4(A) and (B). Rms velocities decrease with increase in the polymer concentration with higher values near the impeller tip and lower values near the vessel wall. Radial rms velocities close to the tip in 10 000 ppm solution differ significantly from those in other concentrations at the corresponding locations. Along the radial plane at $z = -0.36R_i$ (Fig. 5(A)), radial rms velocities are maximum near the vessel wall and axial rms velocities (Fig. 5(B)) are maximum between $r = 1.6$–$2R_i$. The rms values for 10 000 ppm solution are

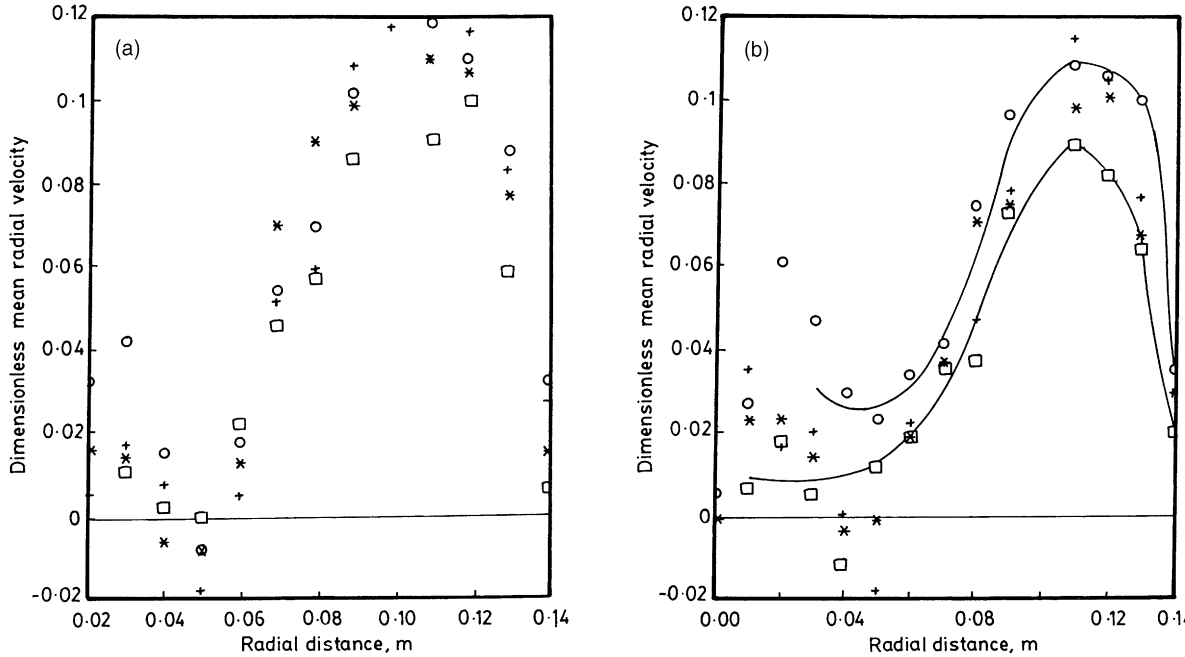


Fig. 3. (A) Radial profile of mean radial velocity at $z = 0.36R_i$. (B) Radial profile of mean radial velocity at $z = -0.36R_i$.

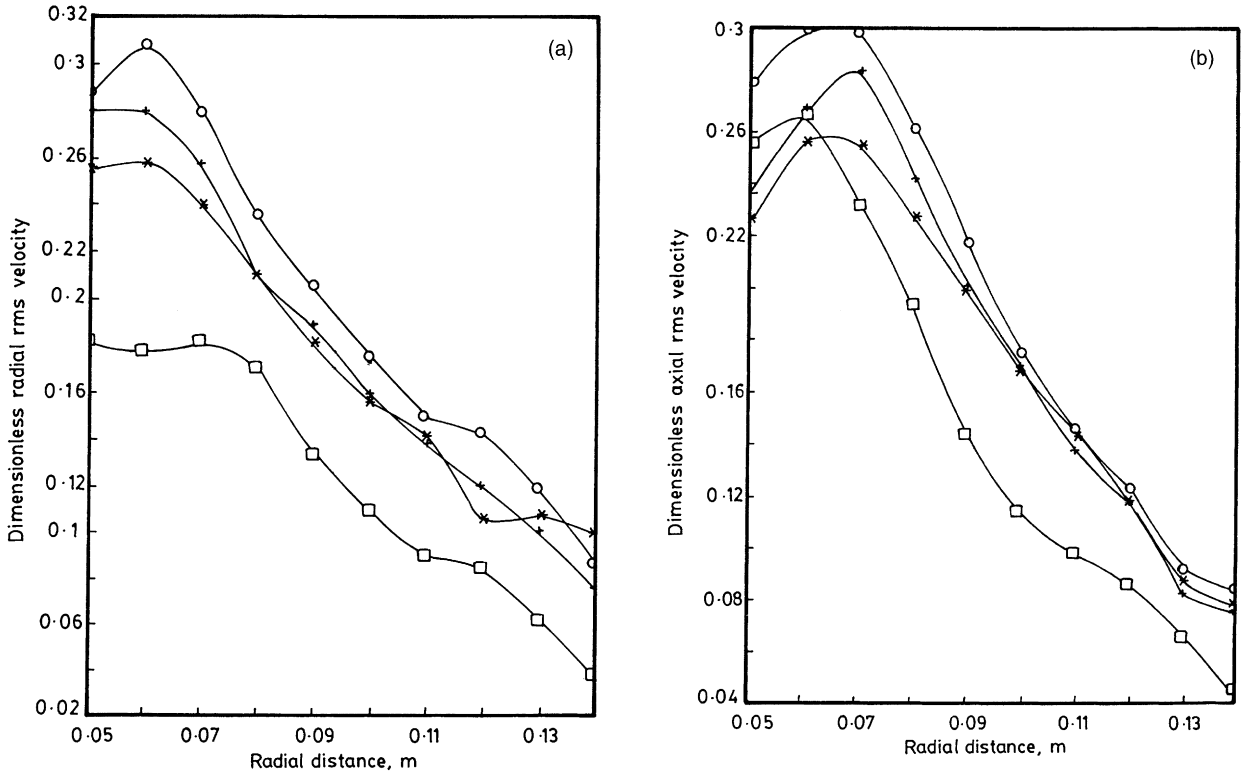


Fig. 4. (A) Radial profile of radial rms velocity at $z = 0$. (B) Radial profile of axial rms velocity at $z = 0$.

far lower than corresponding values in other concentrations and the magnitude does not vary much in the radial direction. The suppression of turbulent fluctuations was also observed by Pinho and Whitelaw [5] in fully developed pipe flows of CMC.

### 3.1.2. Flow in the bulk of the vessel

To study the flow in the bulk of the vessel, measurements were made in radial planes at various axial levels and the one at $z = \pm 1.8\ R_i$ is described here. At $z = 1.8R_i$, the radial velocities are inward (Fig. 6(A)). The velocities are very

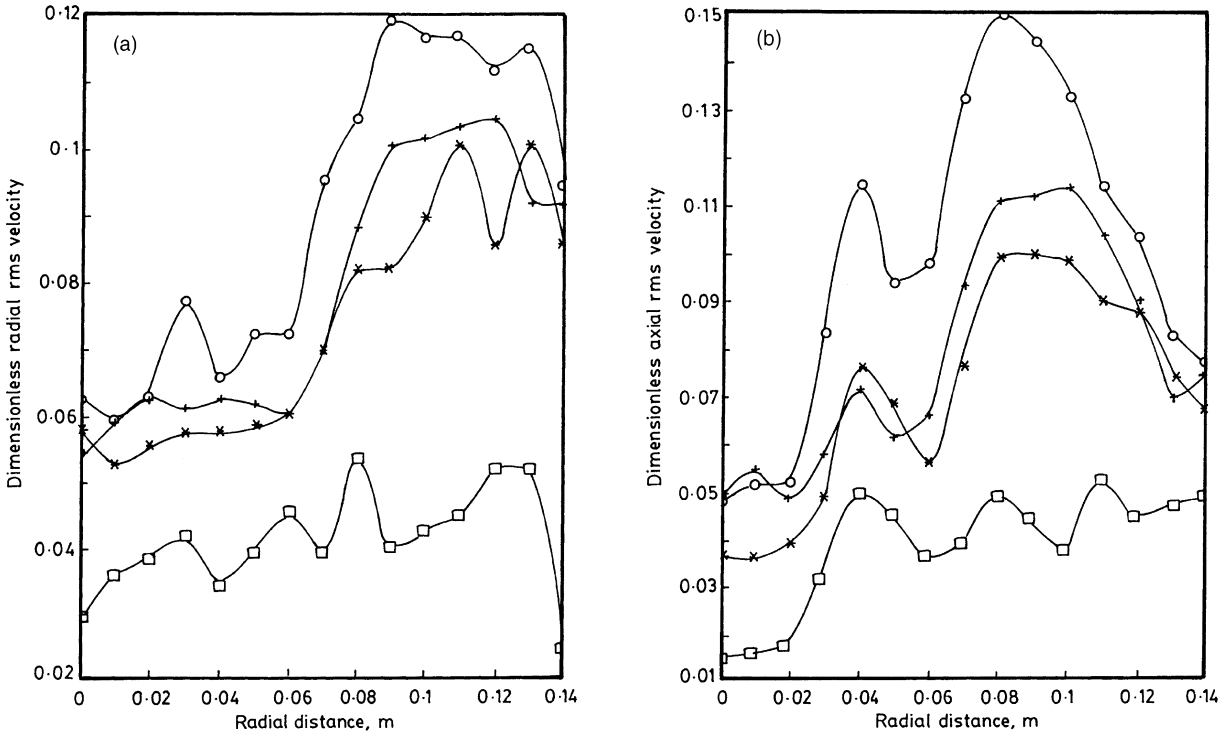


Fig. 5. (A) Radial profile of radial rms velocity at $z = -0.36R_i$. (B) Radial profile of axial rms velocity at $z = -0.36R_i$.

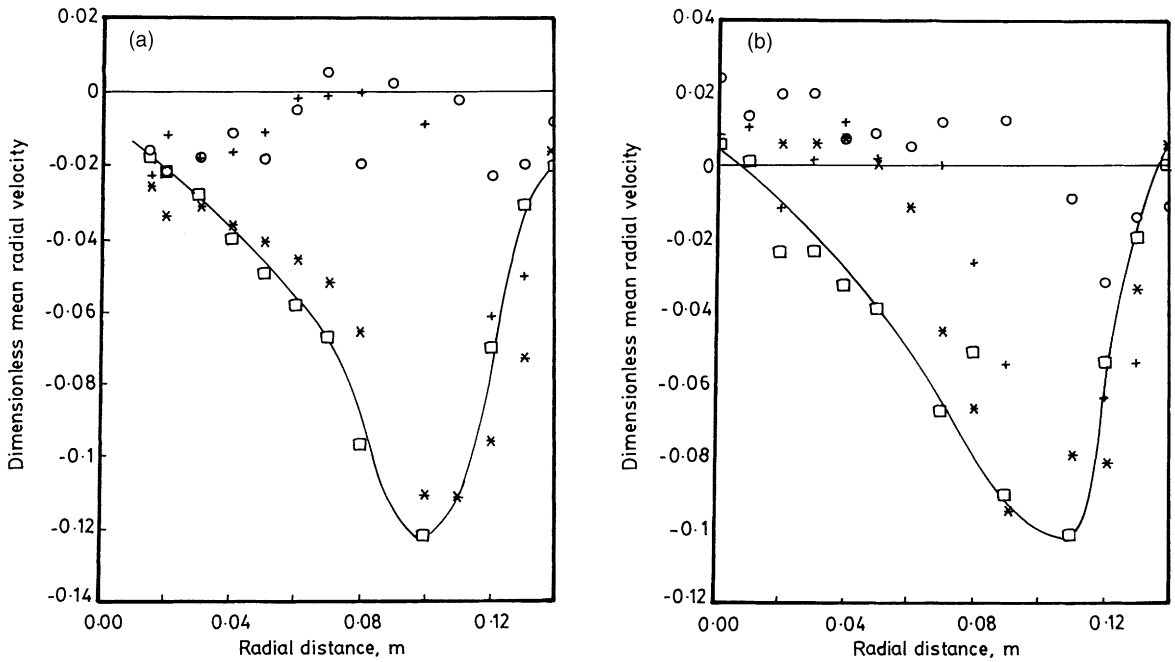


Fig. 6. (A) Radial profile of mean radial velocity at $z = 1.8R_i$. (B) Radial profile of mean radial velociy at $z = -1.8R_i$.

high in case of 5000 and 10 000 ppm solutions and the maximum velocities in these solutions are $0.12V_t$ and $0.115V_t$, respectively, and occur at $r = 2R_i$. For water and the dilute solution, the velocities are very low throughout the radial line. Near the impeller shaft and the vessel wall, the velocities are very close. At $z = -1.8R_i$ (Fig. 6(B)), below the impeller centre plane, again the velocities are higher for higher concentrations but the velocity profiles are far different from those at $z = 1.5R_i$. In all the cases, there is outward flow near the vessel centre and this difference is perhaps due to the absence of impeller shaft and the presence of the vessel bottom. The maximum velocities in 5000

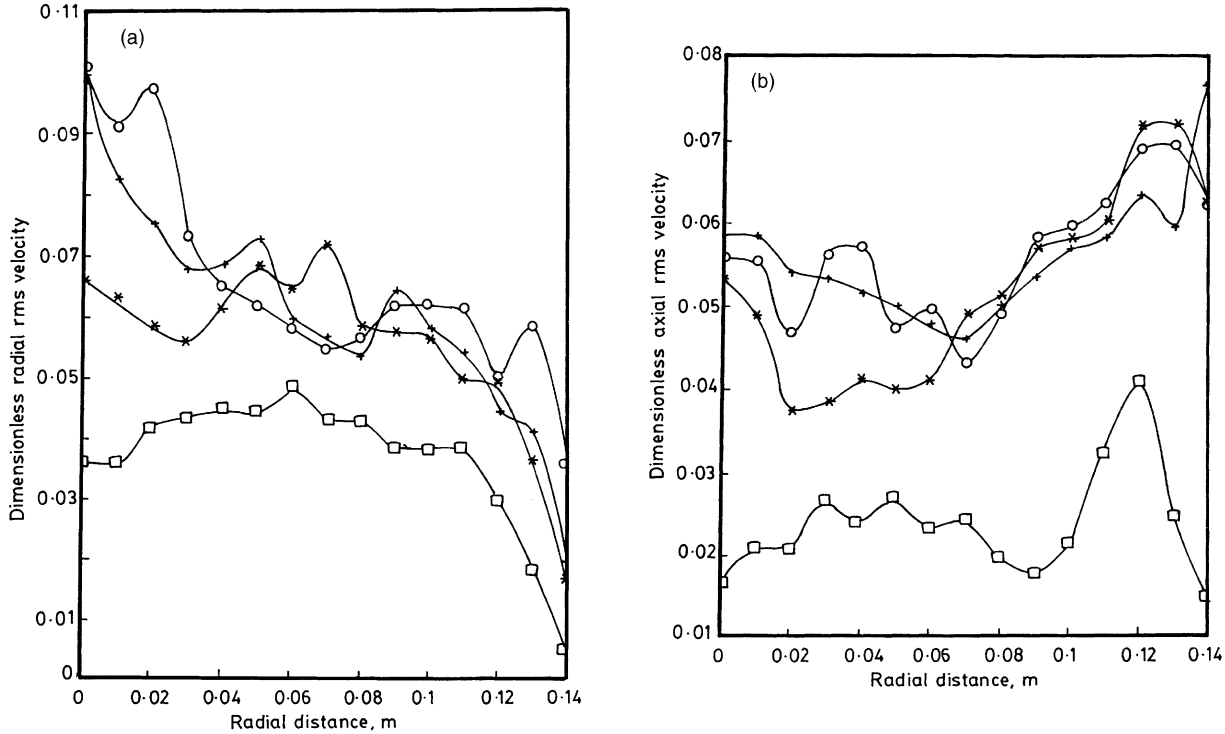


Fig. 7. (A) Radial profile of radial rms velocity at $z = -1.8R_i$. (B) Radial profile of axial rms velocity at $z = -1.8R_i$.

and 10 000 ppm solutions are similar to those above the impeller at $z = 1.8R_i$. But, the velocities for water are very low at this level also. Radial velocities in higher concentration solutions are higher because, at higher concentrations, the circulation loops are shorter vertically as compared to those in lower concentration solution or water and hence, at higher concentrations, $z = 1.8R_i$ is very close to the lower periphery of the lower circulation loop and $z = 1.8R_i$ is close to the upper periphery of the upper circulation loop where the flow is mainly radial. In water, the circulation loops extend almost upto the vessel bottom and upper surface of water from the impeller centre plane.

Rms velocities in the bulk were found to decrease with an increase in the polymer concentration. At $z = -1.8R_i$, radial profile of axial rms velocities is different from that of radial rms velocities. Radial rms velocities are minimum near the vessel wall (Fig. 7(A)), whereas, the axial rms velocities are higher near the vessel wall (Fig. 7(B)). Again, the rms velocities decrease with increase in the polymer concentration. Very low values of axial rms velocities in the case of 10 000 ppm solution is perhaps due to the reason that at this level the axial velocities are very low and flow occurs smoothly in the radial direction.

Vector diagrams of the flows in $r$–$z$ coordinates at all concentrations are shown in Fig. 8(A–D). Circulation loops are seen and change in size with increasing concentrations is quite clear.

Primary and secondary flow numbers were calculated using the following expressions:

Primary flow number,

$$N_q = \frac{Q}{ND^3} \tag{1}$$

Secondary flow number,

$$N_{qs} = \frac{Q_s}{ND^3} \tag{2}$$

where,

$$Q = \pi D \int_{-B_w/2}^{+B_w/2} U(z)\,dz \tag{3}$$

$$Q_s = \pi D \int_{-z_r}^{+z_r} U(z)\,dz \tag{4}$$

$B_w$ is the impeller blade height and $z_r$ is the point of reversal of radial velocity in the vertical plane. Flow numbers at all the concentrations are given in Table 2. The flow numbers decrease with an increase in the polymer concentration. This is due to the decrease in the Reynolds number with an increase in the polymer concentration. This decrease in Reynolds number results in the increase of average resultant length scale in the bulk as polymer concentration increases ($z = \pm 1.8R_i$, Fig. 9(A) and (B)).

The values of power number are given in Table 3. It can be seen that the power decreases with an increase in the

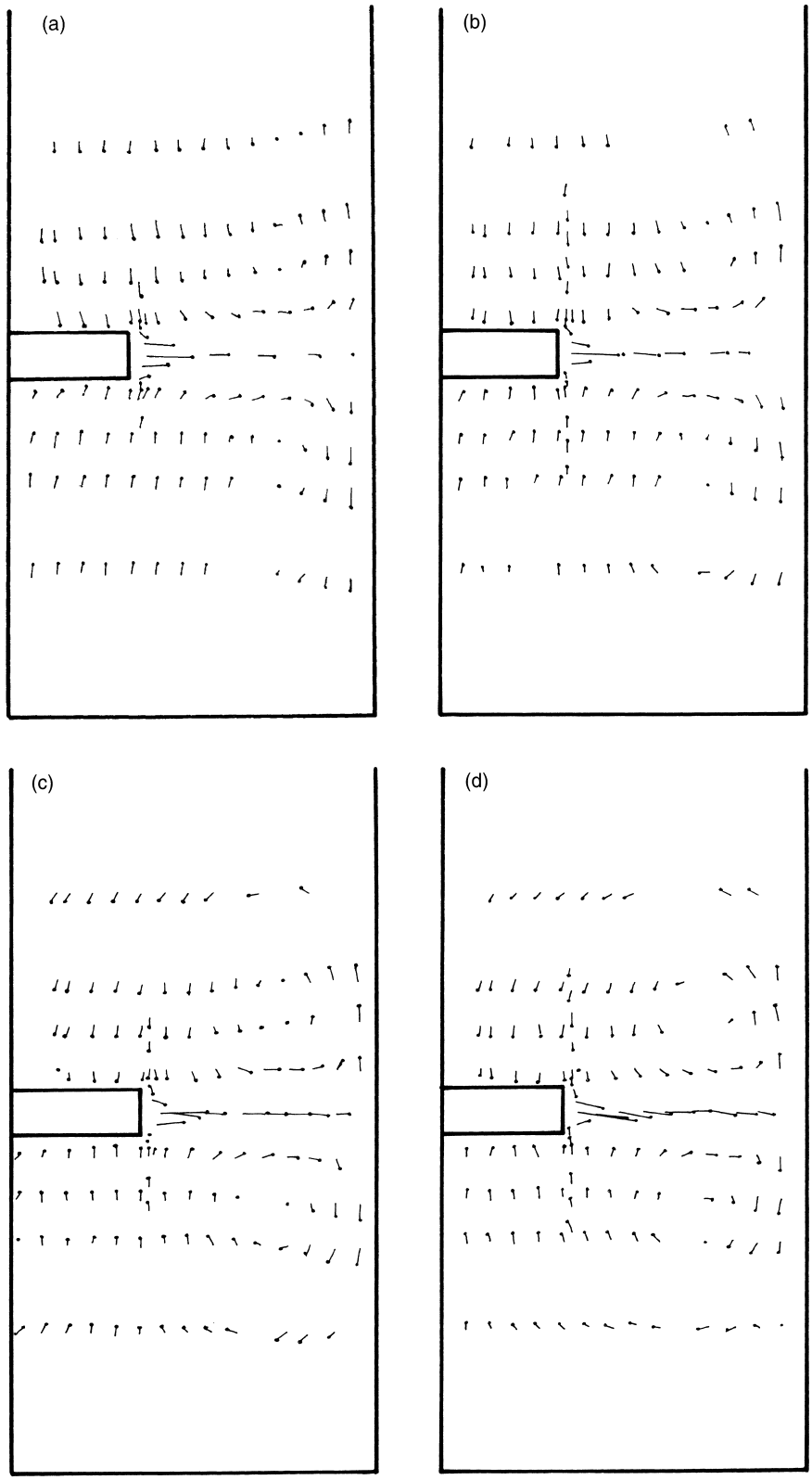


Fig. 8. (A) Flow generated by disc turbine in water. (B) Flow generated by disc turbine in 2000 ppm PAA solution. (C) Flow generated by disc turbine in 5000 ppm PAA solution. (D) Flow generated by disc turbine in 10 000 ppm PAA solution.

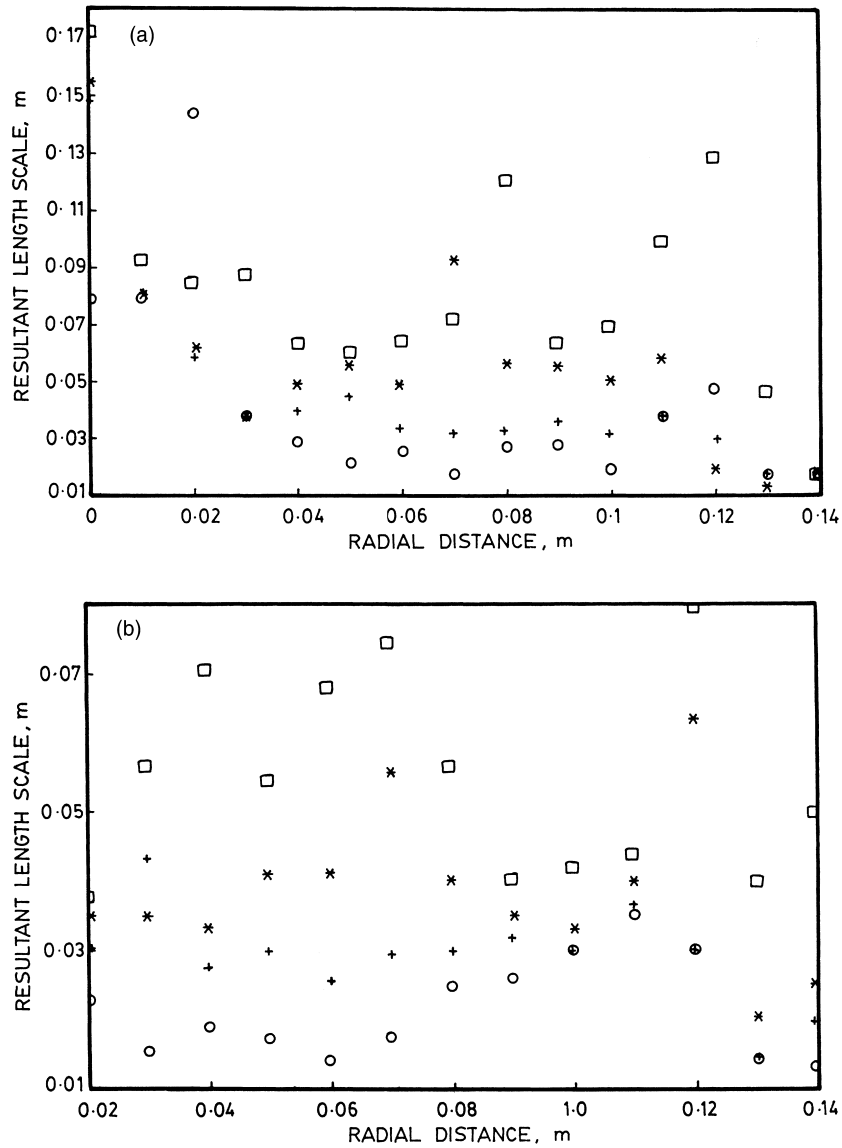


Fig. 9. (A) Radial profile of resultant length scale at $z = -1.8R_i$. (B) Radial profile of resultant length scale at $z = 1.8R_i$.

Table 3
Energy balance details for different concentration solutions

| PAP concentration (ppm) | Input rate (W) | $\epsilon_T$ (W) | Impeller power number ($N_p$) | Power number on the basis of turbulent energy dissipation rate |
|---|---|---|---|---|
| 0 (water) | 4.52 | 4.36 | 4.97 | 4.78 |
| 2000 | 4.51 | 3.28 | 4.95 | 3.59 |
| 5000 | 3.53 | 2.27 | 3.88 | 2.49 |
| 10 000 | 3.2 | 1.37 | 3.51 | 1.50 |

polymer concentration. It may be noted that even though the Reynolds number (Table 2) decreases with an increase in the polymer concentration, the power number does not increase according to the usual $N_p$–Re relationship. This indicates the extent of drag reduction in the presence of polyacrylamide. Similar observations have also been made by Ranade and Ulbrecht [8]. They have measured the power consumption of a disc turbine in viscous Newtonian and viscoelastic non-newtonian liquids (PAA solutions) with and without aeration in the transition regime. It was observed that without aeration viscoelastic liquids exhibit a lower power consumption than the inelastic liquids. They

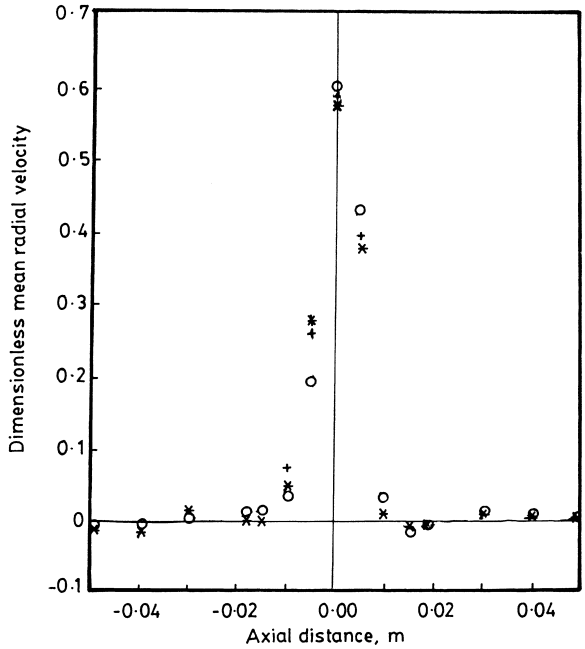


Fig. 10. Axial profile of mean radial velocity at $r = R_i + 3$ mm Symbols: (○), 4.5 r s$^{-1}$; (+), 7.66 r s$^{-1}$; (∗), 1.66 r s$^{-1}$ (from Figs. 10–13).

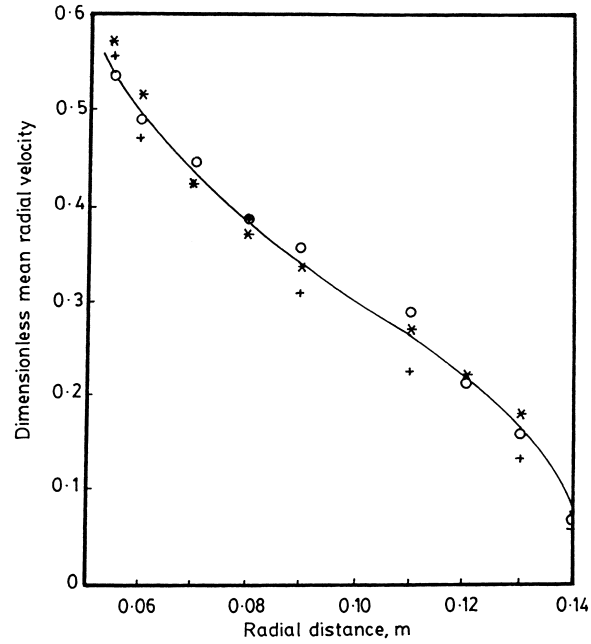


Fig. 11. Radial profile of the mean radial velocity at $z = 0$ (effect of impeller speed).

have reported that the power number decreases as the concentration of PAA increases. It is reasoned that in the transition regime, since the inertia starts influencing the flow regime, both elasticity and pseudoplasticity would reduce the power consumption. They have stated that the separation of the two influences is difficult. Quraishi et al. [9] also observed similar reductions in torque in turbulent dilute polymer solutions, which were slightly elastic.

### 3.2. Effect of impeller speed

In addition to impeller speed of 4.5 r s$^{-1}$, flow measurements were also made at 1.6 r s$^{-1}$ and 7.33 r s$^{-1}$ in 5000 ppm solution in order to study the effect of impeller speed on the flow generated. Along the vertical periphery of the impeller, the axial profiles of radial velocities (Fig. 10) appear to be same at all the three impeller speeds. Also, radial profiles of mean radial velocities along the impeller centre line (Fig. 11) are similar at all the speeds. Hence, in the impeller vicinity, the dimensionless mean velocities are independent of the impeller speeds in the range of 1.6 to 7.33 r s$^{-1}$. However, at axial level $z = -1.8R_i$, below the impeller centre plane, dimensionless mean radial velocities are lower at lower impeller speeds upto $r = 1.5R_i$. Thereafter, they becomes independent of impeller speed (Fig. 12). At this level, the dimensionless axial velocities were very low at lower speeds. In the bulk, the length of the loops increase with an increase in speed due to shear thinning. Therefore, at low rad s$^{-1}$, the level $z = -1.8R_i$ lies at the lower periphery of the circulation loop where radial velocities are totally inward and axial velocities are very low.

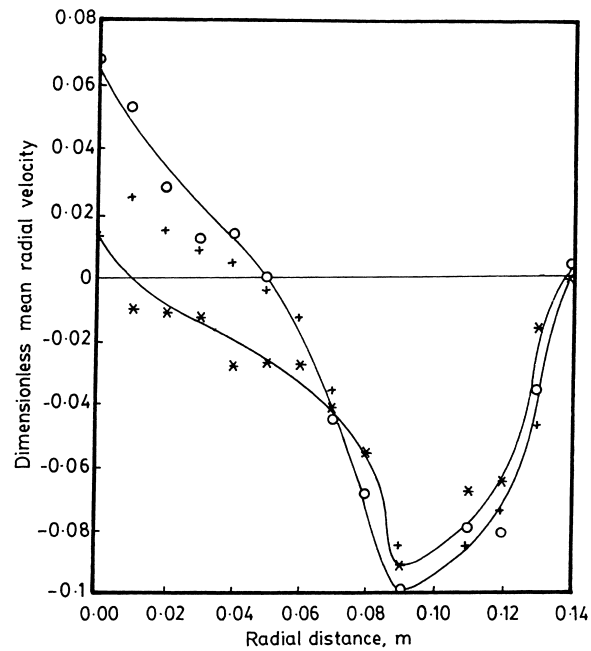


Fig. 12. Radial profile of mean radial velocity at $z = -1.8R_i$ (effect of impeller speed).

### 3.3. Energy balance

Energy balance has been established by integrating the local values of turbulent energy dissipation rate ($\epsilon$), which is found from the following equation:

$$\epsilon = \frac{u'3}{L} \tag{5}$$

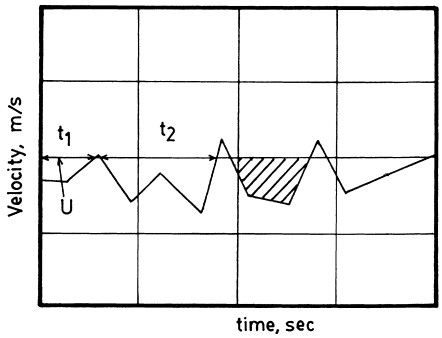


Fig. 13. Velocity profile showing eddies of different life times.

Where $u'$ is characteristic velocity scale and $L$ is characteristic length scale.

In the present work, resultant rms velocity has been considered as the characteristic velocity scale. Length scale has been found using the approach of Luk and Lee [10]. Consider a typical velocity profile as shown in Fig. 13. $t_1$ and $t_2$ are the time spent by the eddies at the measurement point. If $u_1$ and $u_2$ are the velocities of the respective eddies in the radial direction then,

$$L_{1x} = u_1 t_1 \tag{6}$$

is the distance travelled by the first eddy in the radial direction. This distance $L_{1x}$ is taken as the radial length-scale of the first eddy.

The turbulent kinetic energy of the first eddy in the radial direction is

$$k_{1x} = \frac{1}{2} u_1^2 \tag{7}$$

$$u_1 = \sqrt{2k_{1x}} \tag{8}$$

substituting Eq. (8) in Eq. (6) we get

$$L_{1x} = \sqrt{2k_{1x}}\, t_1 \tag{9}$$

Similarly length-scale is calculated in the axial direction and the resultant is taken as the characteristic length scale of the first eddy.

$$L_1 = \sqrt{L_{1x}^2 + L_{1y}^2} \tag{10}$$

Such an exercise is carried out for all the eddies present in the velocity profile and the average length scale is found by time weighting. The average length-scale is used in finding the local turbulent energy dissipation rate.

The energy input rate by the impeller is given by:

$$P = N_p \rho N^3 D^5 \tag{11}$$

The total energy dissipation rate ($\epsilon_T$) in the vessel can be calculated on the basis of local turbulent energy dissipation rates

$$\epsilon_T = \int_0^R \int_0^z \int_0^{2\pi} \epsilon r \, dr \, dz \, d\theta \tag{12}$$

It can be seen from Table 2 that flow is in turbulent regime for the case of water. Under these conditions the energy supplied by the impeller Eq. (11) almost equals the total turbulent energy dissipation rate Eq. (12). On the basis of this relation the power number for disc turbine works out to be 4.78 (Table 3) which is in excellent agreement with the measured value of 4.97. Similar procedure was used for 2000, 5000 and 10 000 ppm PAA solutions. The power numbers were found to be 3.59, 2.49 and 1.5 against the measured power numbers of 4.95, 3.88 and 3.51. It can be seen that the estimated power number is less than the measured power number and the difference increases with an increase in the polymer concentration. It may be pointed out that the estimated power number considers only the turbulent energy dissipation rate and it is expected that the contribution of turbulent energy dissipation should decrease with a decrease in the Reynolds number (Table 2).

## 4. Conclusions

Axial and radial components of velocities generated by standard disc turbine in polyacrylamide solutions of three different concentrations in vertical cylindrical tank have been measured. In the impeller stream, mean flow was found to be the same for all the concentration solutions. But turbulence gets suppressed greatly for 10 000 ppm solution. In the bulk, length of the circulation loop decreases with increase in polymer concentration. Since, in the impeller stream, no sudden reduction was noticed in radial velocities, flow in each case extended fully upto the vessel wall. Primary and secondary flow numbers and power number decreased with an increase in the polymer concentration. In the impeller vicinity, dimensionless mean velocities are independent of impeller speed (in the range of 1.66–7.66 r $s^{-1}$). The values of maximum shear rates were estimated in the impeller region as well as bulk region. On this basis, Reynolds number have been reported. There were found to be in qualitative agreement with the Reynolds number obtained by Metzner–Otto correlation.

A procedure has been given for the estimation of turbulent energy dissipation rate. A complete energy balance has been established for the case of turbulent flow. The turbulent energy dissipation rates were also determined for the polymer solutions where the flow was in the transition regime.

## 5. Nomenclature

| | |
|---|---|
| $B_w$ | Impeller blade height, m |
| BR | Bulk region |
| $D$ | Impeller diameter, m |
| $H$ | Height of liquid in the vessel, m |
| IR | Impeller region |
| $k_{1x}$ | Turbulent kinetic energy of the first eddy in the radial direction, $m^2\ s^{-2}$ |
| $L$ | Characteristic length scale, m $s^{-1}$ |

$L_1$ Resultant length scale of the first eddy in the velocity profile, m $s^{-1}$
$L_{1x}$ Radial component of the length scale of the first eddy in the velocity profile, m
$L_{1y}$ Axial component of the length scale of the first eddy in the velocity profile, m
M–O Metzner and Otto
$N$ Impeller rotational speed, rad $s^{-1}$
$N_p$ Power number
$N_q$ Primary flow number
$N_{qs}$ Secondary flow number
$P$ Power, W
ppm Parts per million
$Q$ Impeller pumping capacity, $m^3$ $s^{-1}$
$Q_s$ Overall circulation rate (primary plus secondary flow), $m^3$ $s^{-1}$
$R$ Radius of the vessel, m
Re Reynolds number
$R_i$ Impeller radius, m
$r$ Radial distance, m
$T$ Vessel diameter, m
$t_1$ Life time of the first eddy in the velocity profile, s
$u$ Radial rms velocity, m $s^{-1}$
$u_1$ Fluctuating component of radial velocity of the first eddy in the velocity profile, m $s^{-1}$
$u'$ Characteristic velocity scale, m $s^{-1}$
$U$ Radial mean velocity, m $s^{-1}$ (positive towards vessel wall and negative towards vessel centre)
$V_t$ Impeller tip velocity, m $s^{-1}$
$w$ Axial rms velocity, m $s^{-1}$
$W$ Axial mean velocity, m $s^{-1}$
$z$ Axial distance (positive above the impeller centre plane and negative below the impeller centre plant)

*Greek letters*

$\epsilon$ Turbulent energy dissipation rate, $m^2$ $s^{-3}$
$\epsilon_T$ Total integrated $\epsilon$, W
$\rho$ Density of water, Kg $m^{-3}$
$\theta$ Tangential coordinate
$\mu_a$ Apparent viscosity, Pa s

## Acknowledgements

VPM and PK are grateful to the University Grants Commission for the award of fellowship. The research work was supported by a grant from the Department of Biotechnology, Government of India (BT/12/11/PRO 485/97-PID)

## References

[1] J.W. Hoyt, Trans. ASME Ser. D. 94 (1972) 258.
[2] P.S. Virk, AIChE J. 21 (1975) 625.
[3] A. White, J.A.G. Hemmings, Drag reduction by additive, BHRA Fluid Engineering, 1976.
[4] F.T. Pinho, J.H. Whitelaw, J. Non-Newtonian Fluid Mech. 34 (1990) 129.
[5] F.T. Pinho, J.H. Whitelaw, J. Fluid Mech. 226 (1991) 475.
[6] M.J. Rudd, AIChE Symp. Series 67 (1971) 21–26.
[7] V.V. Ranade, J.B. Joshi, Chem. Eng. Res. Des. 68 (1990) 19.
[8] Ranade V.R and Ulbrecht, J.J., 1997, Proc. 2nd European Conf. on Mixing, F6-83–F6-100.
[9] A.Q. Quraishi, R.A. Mashelkar, J.J. Ulbrecht, J. Non-Newtonian Fluid Mech. 1 (1976) 223.
[10] S. Luk, Y.H. Lee, AIChE J. 32 (1986) 1546.